



Research Paper

# REMOTE SENSING TO IDENTIFY COPPER ALTERATIONS AND PROMISING REGIONS, SARBISHEH, SOUTH KHORASAN, IRAN

Aref Shirazi<sup>1</sup>, Adel Shirazy<sup>2</sup> and Jalal Karami<sup>3\*</sup>

\*Corresponding Author: Jalal Karami ✉jl.karami@modares.ac.ir

Received on: 20<sup>th</sup> March, 2018

Accepted on: 25<sup>th</sup> April, 2018

In order to reduce operational and field costs, remote sensing studies are used at the initial and general exploration stage. Hence, according to the identification of the Mesgaran copper ore deposit which is the copper potential in the Sarbisheh geological map (on scale 1:100,000), remote sensing methods were used to identify similar regions and to show more areas with this type of potential. In this study, due to the suitability of Aster Images to identify copper alterations various methods of remote sensing such as Band Ratios (BR), False Color Combinations (FCC), Least Square Fitting (LS-Fit), Principal Components Analysis (PCA) and finally Spectral Angle Mapper (SAM) for mapping alterations and promising regions were used. Finally, areas with mineralization and alteration were presented as maps.

Keywords: Remote sensing, Image processing methods, Copper alteration, Mesgaran, SAM, LS-Fit, FCC, PCA, BR

## INTRODUCTION

Remote sensing is the acquisition of information about an object or phenomenon without making physical contact with the object and thus in contrast to on-site observation. Remote sensing is used in numerous fields, including geography, land surveying and most Earth Science disciplines (for example, hydrology, ecology, oceanography, glaciology, geology); it also has military, intelligence, commercial, economic, planning, and humanitarian applications (Schott, 2007; and Guo *et al.*, 2013).

In current usage, the term “remote sensing” generally refers to the use of satellite- or aircraft-based sensor technologies to detect and classify objects on Earth, including on the surface and in the atmosphere and oceans, based on propagated signals (e.g., electromagnetic radiation). It may be split into “active” remote sensing (i.e., when a signal is emitted by a satellite or aircraft and its reflection by the object is detected by the sensor) and “passive” remote sensing (i.e., when the reflection of sunlight is detected by the sensor) (Robert, 2007; Liu and Mason, 2013; and Ran *et al.*, 2017).

<sup>1</sup> AmirKabir University of Technology (Tehran Polytechnic) Mining and Metallurgical Engineering Department Tehran, Iran.

<sup>2</sup> Shahrood University of Technology, Faculty of Mining, Petroleum and Geophysics, Shahrood, Iran.

<sup>3</sup> Assistant Professor, Remote Sensing & GIS Department, Tarbiat Modarres University, Tehran, Iran.

Remote sensing is one of the methods that can be used to separate surface anomalies from the field by detecting alterations and target minerals. In the early stages of regional exploration, it is possible to identify mineralization and alteration by using the classic and modern statistical methods on the geochemical data in the study region (Shirazi *et al.*, 2018). The combination of remote sensing results and geochemical statistical studies can provide more reliable results.

## DATA AND RESEARCH METHODS

### Regional Geological Setting

The studied area is part of the Sarbisheh geological map (on scale 1:100,000) and the Mesgaran copper deposit is located 29 km south of Sarbisheh city. The UTM geographic position is between 0770500 and 0773000 East (longitude) and 3577500 to 3581500 North (latitudes) (Figure 1).

There are no violent heights in this range, and most of them are dipped and plain. Due to the existence of Mafic and Ultramafic units (ophiolite sequence) and erosion function on these units, the topography of the area is a mild and quiet hill (Figure 2). The sedimentary sections of the region, in particular, have more rugged topography of limestone than mineral area. In terms of structural and sedimentary divisions, the study area is a small part of the structural zone of East of Iran and is metallurgically located in the northern part of Ahangaran-Bandaan (Zarjabad *et al.*, 2015; and Aqanabati, 2009).

In terms of lithology, exploratory areas include ultrabasic rocks, diabasic dikes, pillow basalts, calcareous outcrops, phyllite and schist lenses. Travertine can be mentioned from the newest lithological units. this collection is made of porous travertine around travertine springs (Mohammadi *et al.*, 2007) (Figure 3).

The rock units in the region show a complete ophiolite sequence, but because of the

Figure 1: Geolocation of Study Area, Sarbisheh, Southkhorasa Province of IRAN

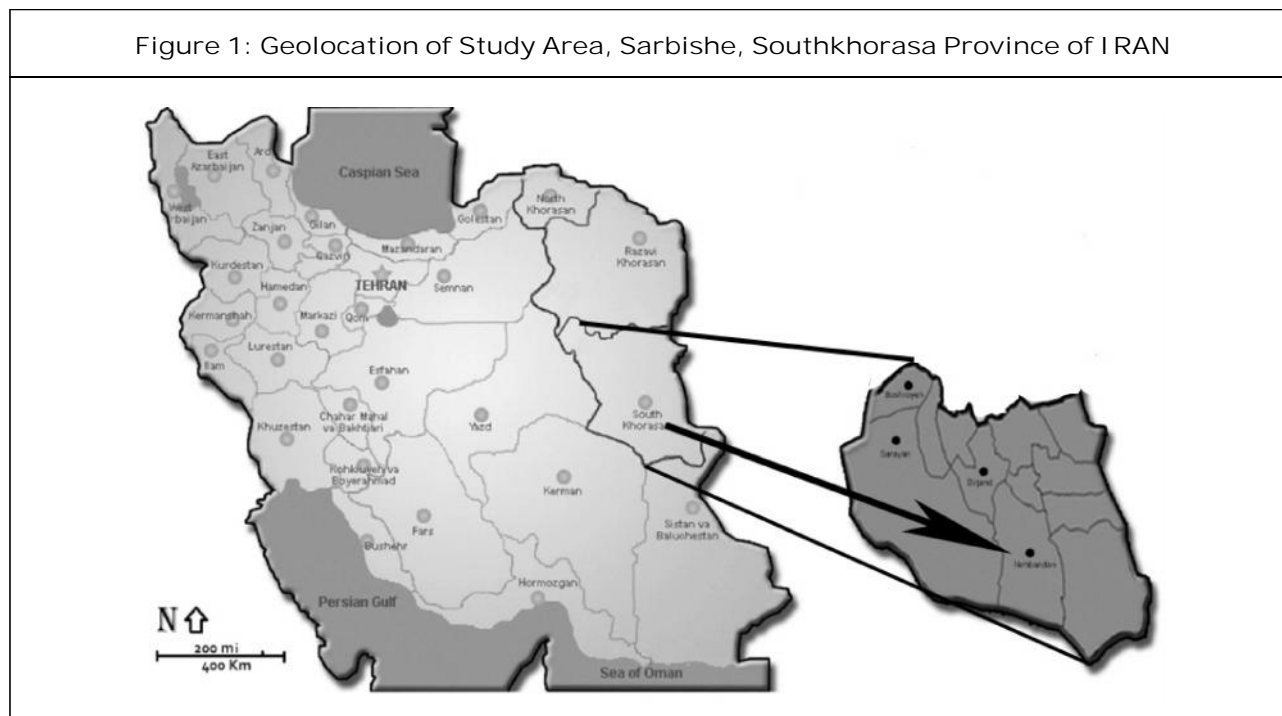


Figure 2: DEM of the Mesgaran Mining Area, Provided by the Quickbird Satellite

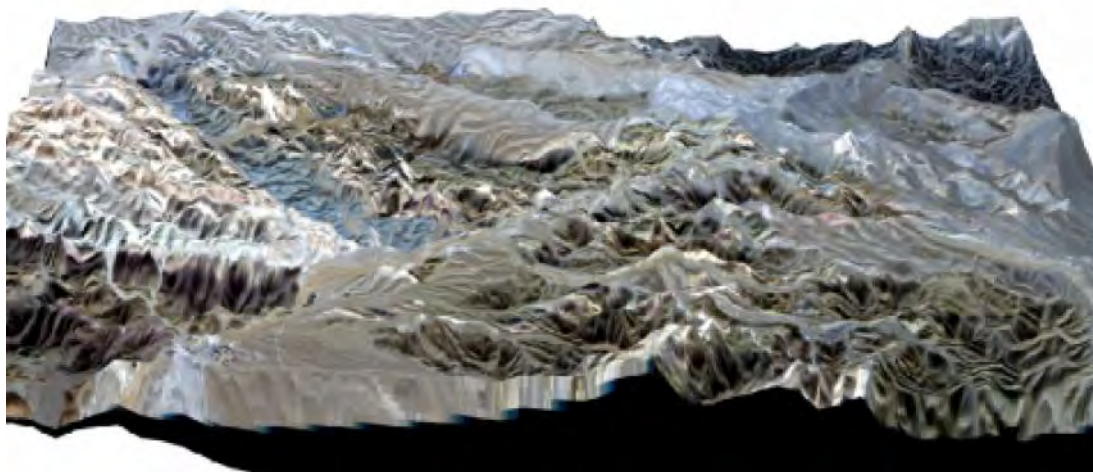
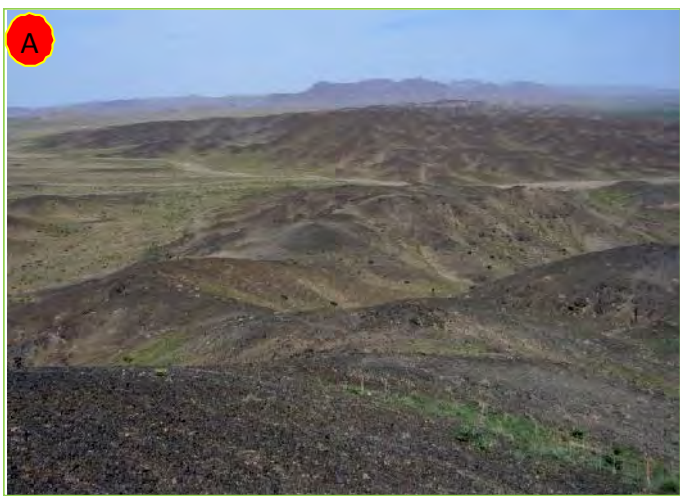


Figure 3: View of the Ophiolite Sequence of the Region, A) Mild Morphology and Hills of Ultrabasic Rocks in the North of Mesgaran, B) A View of Pillow Basalt Whose Outer Surface is Affected by Contact with Sea Water and Cooling and Its Color and Texture have Changed



compressive stresses dominant on the region, the boundaries of these units are largely faultly, and the outcrop of ultrabasic rocks, basic rocks and ocean sediments does not follow any order.

### Mineralization

In Mesgaran mining area Copper mineralization has occurred in pillow-lava and andesite-basalt sequences of eastern Iran. Two mineralization

zones were identified as sulfide mineralization with silicified stockworks (primary mineralization) and supergene mineralization. The primary copper mineralization in this region is mostly in accordance to silicified or carbonate veins with epidote and chlorite in volcanic basalt.

These veins cross out the volcanic complex as stockworks which include Chalcopyrite,

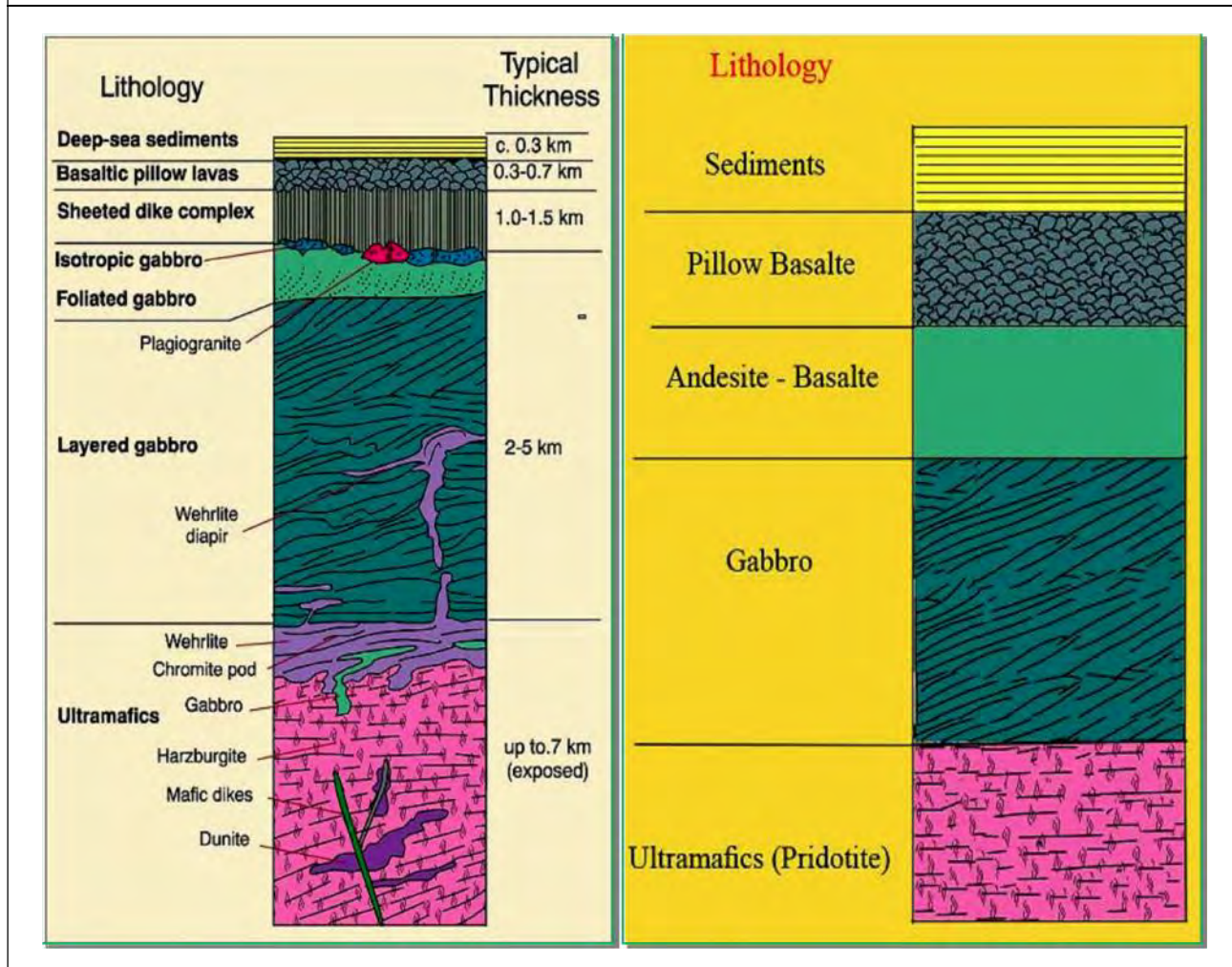
Bournite and Pyrite. In this region, we observed no evidence proving massive deposit or lens shape deposit creation. The main observed minerals are sulfide and oxide forms of copper. Malachite, Azurite and lower amounts of Tenorite and native copper in oxide supergene zone and chalcopyrite and bournite as the primary sulfides have been detected. Oxidation and erosion caused goetite and hematite around sulfide minerals like Chalcopyrite and Pyrite (Figure 4). Alteration is observed almost everywhere on the surface but the degree of alteration varies. Generally alteration occurs when rocks react to hydrothermal and magmatic fluids and this reaction leads to chemical and mineralogic changes. Chlorite alteration has occurred in large scale which is a specific form of Propylitic alteration. Al, Fe and Mg rich fluids caused chlorite alteration in basic rocks (Agharezaei and Hezarkhani, 2016).

In this region, argillic alteration (presence of Montmorillonite mineral) as a secondary alteration process is observed too. Most of the copper is in oxide form on the surface and because of high degree of oxidation and erosion, sulfide mineralization is rare in outcrops so deeper samples are needed to study the deposit. Drilling is the best choice in such situations. According to mineralization and the host rock (pillow lava and andesite-basalt), the mineralization type seems to be categorized as a massive sulfide and redbed type. Generally the mineralization manner (copper mineralization as stockworks), the host rock (pillow lava and andesite-basalt), the deposit development environment (a volcanic part of an Ophiolite sequence) and the alterations (quartz-carbonate, epidote and chlorite) observed in this region and comparing them to the massive sulfide types leads to classify Mesgaran deposit as a Volcanic Massive Sulfide (VMS) type. But

Figure 4: Sulphide Mineralization (Chalcopyrite and Pyrite) in Basalt that has been Converted into Iron Hydroxides, Chalcocites and Covellite by the Supergene Processes



Figure 5: Expression of the Complete Ophiolitic Sequence (Left) and its Comparison with the Existing Parts of the Ophiolitic Sequence of Eastern Iran in the Mesgaran Mining Area (Without Scale) (Right) (Shirazi, 2016)



still more studies are needed to prove this claim with higher accuracy (Agharezaei and Hezarkhani, 2016; and Shirazi, 2016) (see Figure 5).

**Satellite Remote Sensing Data**

In this study, the image of the ASTER Satellite Sensor was used. *ASTER (Advanced Spaceborne Thermal Emission and Reflection Radiometer)* is a high resolution imaging instrument that is flying on the Terra satellite (Arivazhagan and Anbazhagan, 2017). *ASTER* will obtain detailed maps of land surface temperature, emissivity, reflectance and elevation of the Earth.

ASTER has three sensors to measure and record the reflected and emitted Electromagnetic Radiation (EMR). They are working in different wavelength regions the Visible and Near Infrared (VNIR) between 0.52 and 0.86 μm, Short Wave Infrared (SWIR) between 1.6 and 2.43 μm, and Thermal Infrared (TIR) between 8.125 and 11.65 μm. ASTER data consists of 14 spectral bands 3 VNIR, 6 SWIR, and 5 TIR with 15, 30, and 90 m spatial resolution, respectively (Obata et al., 2017). The VNIR, SWIR and TIR wavelength regions provide complementary data for lithological mapping (Amer et al., 2010).

Geometric corrections were made using the satellite ETM<sup>+</sup> satellite image on the study area image. In order to ensure the results, IAR Reflectance radiometric corrections were applied to the region image and the results for applying different types of processes were introduced into ENVI software (Padró *et al.*, 2017; and Shirazi *et al.*, 2018).

### **Band Ratios (BR) Method**

In general, all materials are composed of atoms and molecules with a specific composition (Bransden and Joachain, 2003). Therefore, various materials, depending on the structure, absorb or emit electromagnetic radiation at special wavelengths (Zhao *et al.*, 2015). So that the wavelength curve and radiant energy for each object are unique and this is a clear feature of remote sensing science (Gupta, 2017). The result of dividing the values of the brightness of the pixels in a spectral band into another band is called the band ratio. And as a result, new lighting levels or, in other words, a new image are created. Band ratios method is used to detect complications that are not visible in the image of single bands (Dhara *et al.*, 2017).

This method is applicable to the recognition of the spectral reflection of various phenomena for the appearance of a particular phenomenon. Relative images that are based on the reflection characteristics of altered minerals and by dividing the digital values of a spectral band into another band are important in identifying altered areas (Safari *et al.*, 2017).

In order to determine the alteration areas with respect to the spectral characteristics of the index minerals in any kind of alteration, the bands proportions can be defined. Many band ratios

have been identified for the identification of various types of minerals in the case of ASTER data (Gahlan and Ghrefat, 2018).

The results of applying band ratios method are gray-scale images that alone are not a valid criterion for determining the target areas in the study area. It only identifies the areas most likely to have the desired minerals or, in general, the objects to be searched for. Using false color combinations (RGB images) can be produced that make the interpretation and conclusions based on them more reliable and more practical (Garg *et al.*, 2017).

### **False Color Combinations<sup>1</sup> Method**

The importance of displaying the color combination of images in remote sensing can be considered due to their effectiveness in visual interpretation of various effects. One of the effective methods for identifying and separating various geological units is the False Color Combination (FCC) method (Abdelaziz *et al.*, 2018).

The false color combination is a combination of three different bands combined in Red, Green, and Blue (RGB) colors. If the combined bands of red, green, and blue wavelengths are the visible spectrum of electromagnetic spectrum, the resulting image will be a true color combination. If a different combination of red, green and blue bands or other bands of the electromagnetic spectrum is used, a false color image will be obtained that is not similar to the surface of the earth and its colors (Masoumi *et al.*, 2017).

In making false color combinations it is better to use bands that have less correlation. Since the interaction of different wavelengths of electromagnetic energy is different in dealing with

---

<sup>1</sup> FCC

rock units, the sensitivity of the human eye to minor changes in color is much greater than its sensitivity to changes in black and white images. Choosing the best band combination depends on the target (Yao *et al.*, 2017).

Three images can be combined to make the images visible for viewing in three blue, green, and red wavelengths (original RGB color combinations). In this study, this combination has been used to display several images in a single image and simultaneously display different information from a single point (Hereher and Abdullah, 2017).

Calculation of the Optimum Index Factor amount (OIF) is required to obtain the best false color combination (OIF of the higher color combinative with more information). The formula below shows the OIF calculation method (Razmi *et al.*, 2017).

$$OIF = \frac{\sum_{k=1}^3 S_k}{\sum_{j=1}^3 r_j} \quad \dots(1)$$

**In Formula 1:**  $S_k$  is the standard deviation of the  $k$  band,  $r_j$  is the two-band correlation coefficient of the three-band combination (Abbaszadeh, 2010). Sometimes visually, the false color combinations containing major information are determined by the variety of colors (Hooshyari, 2005).

### Principal Components Analysis (PCA)

One of the methods used to reduce the correlation between multivariate data and increase the distinction is the main component analysis (PCA) method. The purpose of this method is to compress data and eliminate redundant data in order to save time and money. By using the PCA

method, we can replace many independent and correlated variables with a limited number of new variables, which are called principal components and are not interconnected (Manuel *et al.*, 2017). In this way, the dimensions of the problem are reduced. In general, the purpose of this method is to compress all the information contained in a main dataset composed of  $n$  channels into less than  $n$  channels or new components. Finally, the components are used instead of the original data (Wang *et al.*, 2017).

In general, this approach reduces the compatibility between different bands data, and new information is obtained and sent to PC channels. By creating a combination of PC channels and dual-source bands, images can be created to illustrate the effects. This technique is a eigenvectors based method, using eigenvalues and eigenvectors, identifies directions with maximum variability and then decreases the dimensions of variables by defining new variables that are linear combinations of the initial variables (Gómez-Palacios *et al.*, 2017). New variables that are the product of the linear combination of initial variables do not show correlation between themselves (Hassanipak and Sharafeddin, 2005).

To compute the main components, at first the variance, covariance, or matrix of correlation between the bands are formed and then eigenvalues and eigenvectors of this matrix are calculated. Because covariance is dependent on the unit of measurement of data and the bands of different bands do not have the same reflexion unit, it is better to use the correlation matrix (Soe *et al.*, 2005).

For each principal component, an image is calculated from its eigenvectors. The numerical values of the principal component image are

calculated using the values of numerical values in the initial images and the components of the eigenvectors as follows:

$$r = \text{Cos}^{-1} \left[ \frac{\sum_{i=1}^{nb} x_i r_i}{(\sum_{i=1}^{nb} x_i^2)^{\frac{1}{2}} (\sum_{i=1}^{nb} r_i^2)^{\frac{1}{2}}} \right] \quad \dots(2)$$

**In Formula 2:**  $P_k$  is the numerical value of the desired pixel for the  $k$ th principal component, DN (i) The numeric value of the  $i$ -th band for the desired pixel,  $a_{ik}$  is the amount of the load obtained from the eigenvectors of the  $k$  component in the  $i$ -th band. Thus, for each principal component or eigenvectors, an image is obtained that represents the variability in its direction (Vincent, 1997).

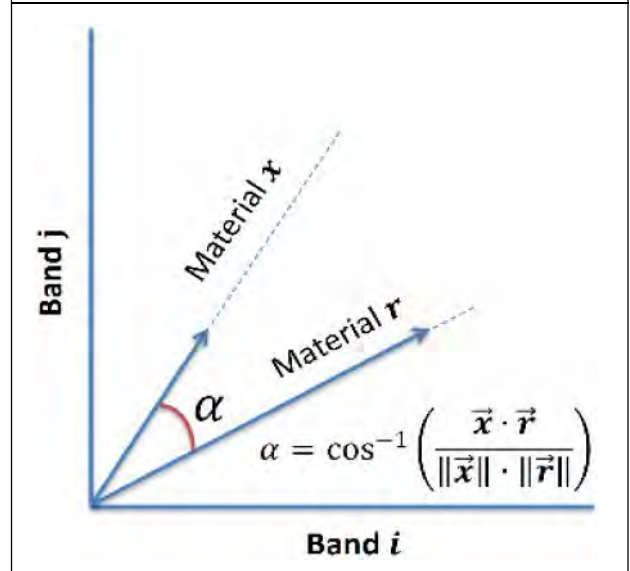
**Least Square Fitting (LS-Fit) Method**

In the regression least squares method, a band is estimated based on the linear combination of other bands using the least squares of errors (Asadzadeh and de Souza Filho, 2016). In this method, the band of the mineral in question is high in adsorption with the rest of the bands, will be divided and the best areas will be detected with pixels containing those minerals (Ezzati et al., 2014; and Ramezanali et al., 2017).

**Spectral Angle Mapper (SAM) Method**

Spectral Angle Mapping (SAM) method is an image classification method by calculating the similarity between the image spectrum and a reference spectrum (e.g., spectral libraries). The algorithm of this method calculates the similarity between two spectra by the spectral angle between them (Hasan et al., 2016). In fact, by transforming the spectra into a vector in a space in the number of dimensions of the bands, the angle between the two vectors is calculated (see Figure 6) (Markovskiy, 2014).

Figure 6: Example of SAM Classification in Case of 2 Spectral Bands, Scalar Product Between Unknown Material x and Library Sample r (Markovskiy, 2014)



In this method, the direction is important for calculating vectors, not length. Therefore, other factors are not considered in this method. In fact, the more the angle (between 0 and 1) is less, the more accurate it will be. If the value is 0, the whole image is identified as the desired phenomenon. To compare a pixel, the desired pixel spectrum is plotted from the examined area with the same pixel spectrum in the laboratory (library) on two bands in a coordinate axis. Then the points are connected to the coordinate center, and the angle between the two lines is used as the pixel identification angle. If the  $n$  bands are used to identify the phenomenon concerned, the following formula is used to obtain an angle (Esmaeeli et al., 2012).

$$r = \text{Cos}^{-1} \left[ \frac{\sum_{i=1}^{nb} x_i r_i}{(\sum_{i=1}^{nb} x_i^2)^{\frac{1}{2}} (\sum_{i=1}^{nb} r_i^2)^{\frac{1}{2}}} \right] \quad \dots(3)$$

**In Formula 3:**  $nb$  is the number of bands. unknown material  $x$  and library sample  $r$ .



## RESULTS AND DISCUSSION

In this section, the results of each of the remote sensing methods which are described in the previous section are presented.

### Band Ratios (BR) Method

In this method on the ASTER images, alive vegetations is red, which is bright or dark, indicates the health of the plants. man-made phenomena, like buildings, are bright blue or gray soils are varied in color, depending on the color of the material, and the water is very dark. Prior to any analysis to distinguish between different rock units and alterations, the vegetation of the region should be identified, due to the presence of different types of clay in these areas. This causes the interference of these areas with the alteration zones and, as we will see, alterations are also seen in red. To determine the vegetation, the band ratio  $(2-3)/(2+3)$  and color combination RGB = 231 were used (Ranjbar *et al.*, 2004; and Kalinowski and Oliver, 2004). After applying the stretch, the image appears as Figure 7.

As shown in the picture above, in the northeastern part of the vegetation cover is a type of agricultural land and in the southern part of vegetation is sporadic.

### False Color Combinations Method

Experimental analyzes have shown that the image with the combination of RGB = 468 is the most suitable color combination for the identification of alteration regions in porphyry copper ore deposits (Ferrier *et al.*, 2002; and Abbaszadeh and Hezarkhani, 2010). Regarding the type of ore deposit studied, the presence of alterations has the potential to determine other potentialities of the region. For example, the presence of chlorite in this type is very significant. In this image, regions with propylitic alteration in green and regions with a phyllic alteration in pinkish yellow are seen (Figure 8). This is due to the high reflectivity of the alunite, kaolinite and muscovite minerals in band 4 compared to the bands 6 and 8 (Ghannadpoor *et al.*, 2012).

Figure 7: Band Ratio  $(2-3)/(2+3)$  (Off Pixels) (Right Image), Color Combination RGB = 231 to Detect Vegetation (Green Pixels) (Left image)

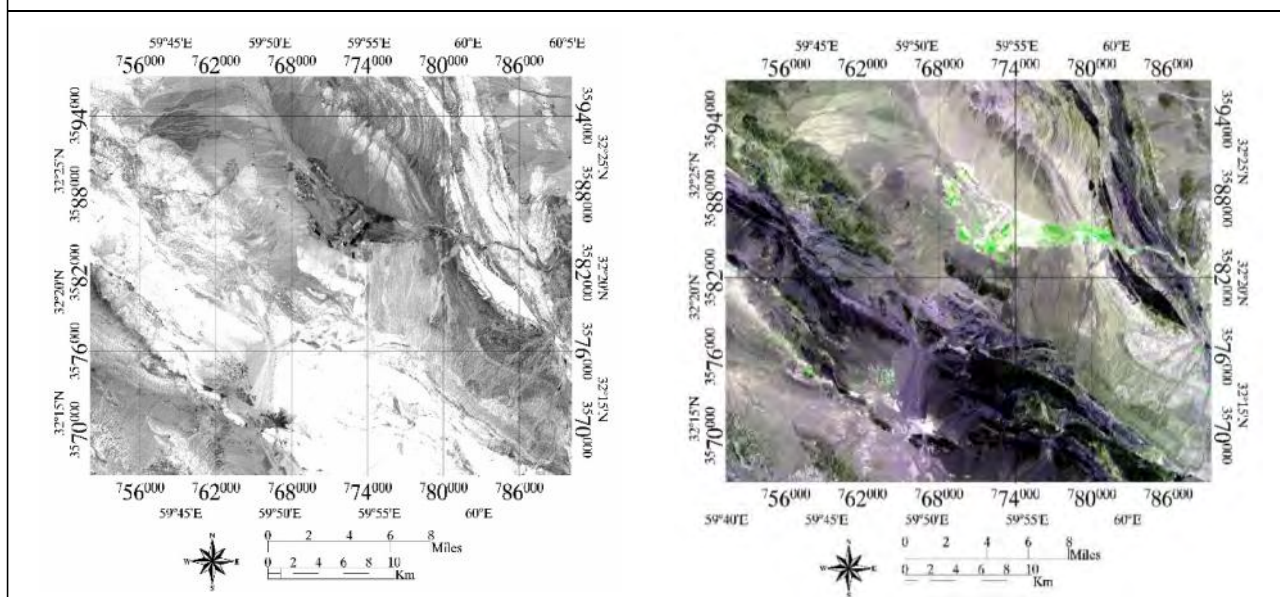
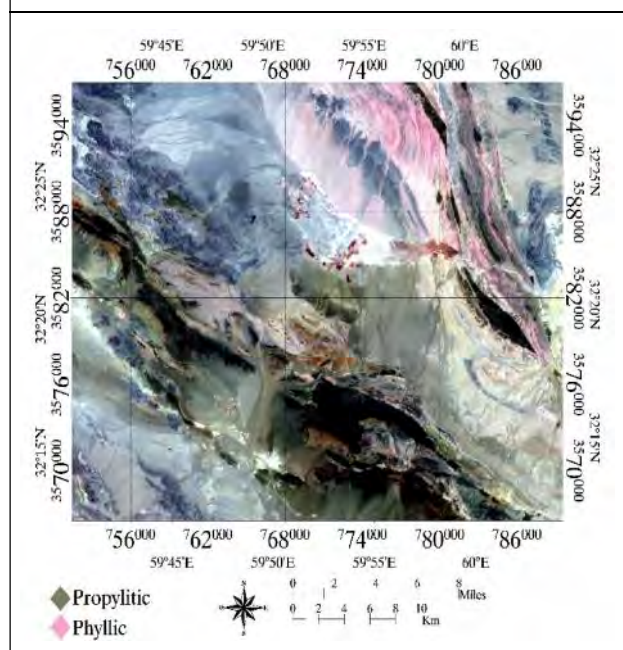


Figure 8: Color False Image with RGB = 468



In Figure 8, the study area is clear in the south of the agricultural land, and it can be seen that there is a proliferation alteration in the mineral area and other southern regions. Vegetation also is not recognizable for the reasons mentioned.

### Principal Components Analysis (PCA)

In this study, we have tried to demonstrate the ability of the Crosta method to use ASTER satellite data. Therefore, the 9 band VNIR + SWIR of the sensor is used to apply the Crosta method. In this way, we have formed a subset of 4 bands for the alterations to be made (Table 1). Then, using the PCA, the eigenvectors matrix for these subsets was calculated to determine the PC containing the target mineral information (hereafter, the desired alteration).

The proper condition for selecting suitable PCs is that in the matrix of eigenvectors, the bands of absorption and reflection of the target minerals simultaneously have the highest values, while these values are non-signs (one negative and the other positive) (Crosta *et al.*, 2003).

Table 1: Bands of the VNIR + SWIR Range, Used to Determine the Alteration Zones in the Mesgaran Area Using the PCA Method (Ferrier *et al.*, 2002)

	The Studied Alterations		
	Propylitic	Phyllic	Argillic
ASTER bands	1	1	1
	4	6	4
	5	7	6
	8	9	7

By using this method, the eigenvectors matrix of each alteration in the region was calculated. The loading coefficients of the selected principal components analysis for propylitic, phyllic and

Table 2: The Loading Coefficients of the Selected Principal Components Analysis for Propylitic Altration

Eigenvectors	Band 1	Band 2	Band 3	Band 4
PC1	0.699650	0.703964	-0.112499	0.047622
PC2	0.405672	-0.333906	-0.268438	-0.780181
PC3	0.415158	-0.520724	-0.413738	0.620734
PC4	0.416610	-0.280341	0.862616	0.061150

Table 3: The Loading Coefficients of the Selected Principal Components Analysis for Phyllic Altration

Eigenvectors	Band 1	Band 2	Band 3	Band 4
PC1	0.702746	0.679851	-0.155281	-0.140846
PC2	0.425999	-0.621416	-0.633743	-0.175320
PC3	0.407799	-0.343625	0.729535	-0.428253
PC4	0.397961	-0.183210	0.205028	0.875228

Table 4: The Loading Coefficients of the Selected Principal Components Analysis for Argillic Altration

Eigenvectors	Band 1	Band 2	Band 3	Band 4
PC1	0.699965	0.668035	-0.226173	-0.112357
PC2	0.405843	-0.310959	-0.087187	0.854982
PC3	0.425100	-0.658958	-0.391580	-0.481382
PC4	0.405747	-0.151024	0.887643	-0.157010

argillic alterations are shown in the Tables 2, 3, 4, respectively.

Based on the contents of the above tables and according to the conditions mentioned above for choosing the appropriate PCs, PCs 3, 4 and 4, respectively, are selected for the study of

Figure 9: The Image Obtained by Crosta Method for Showing Propylitic Alteration (Off Pixles)

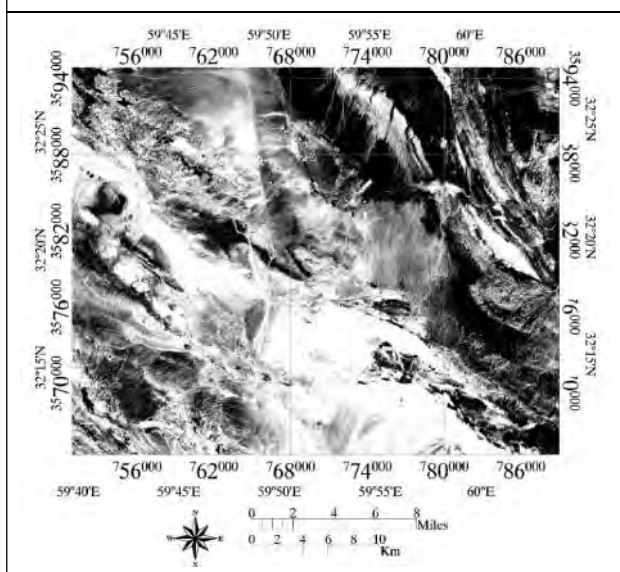


Figure 10: The Image Obtained by Crosta Method for Showing Phyllic Alteration (Bright Pixles)

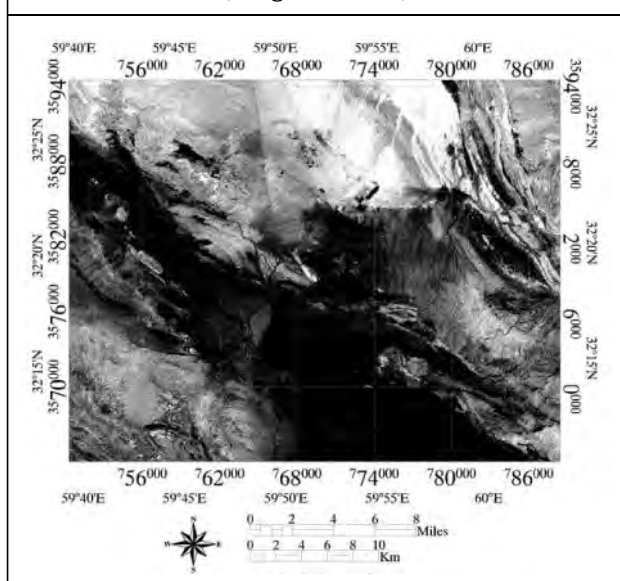
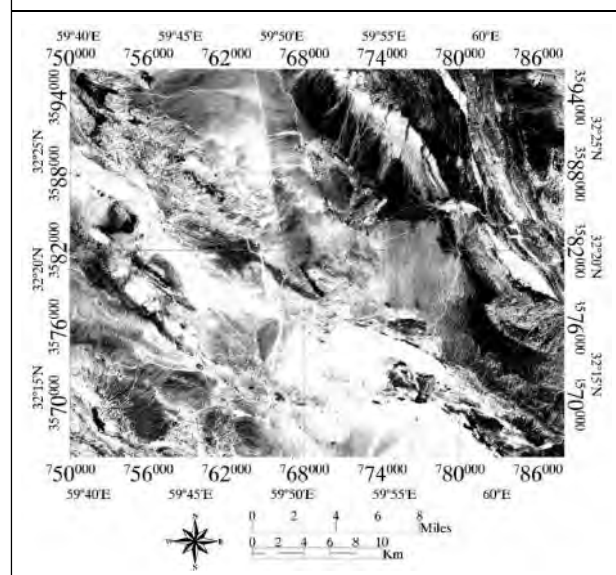


Figure 11: The Image Obtained by Crosta Method for Showing Argillic Altration (Off Pixles)



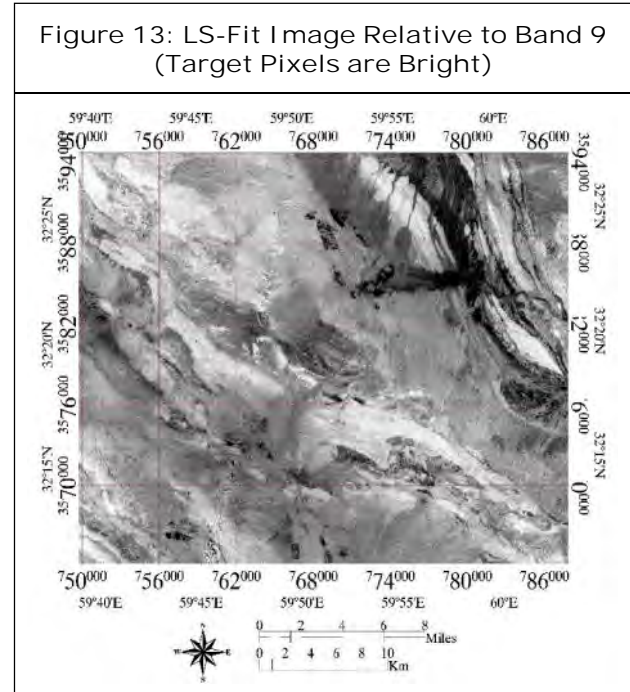
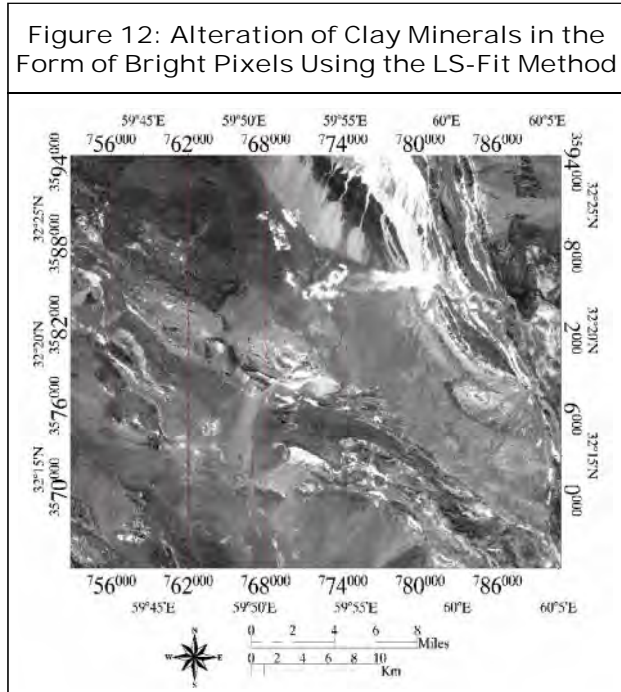
propylitic, phyllic and argillic alterations. The images created by the Crosta method are shown in Figures 9, 10 and 11 respectively for the determination of three propylitic, phyllic and argillic alterations.

From the Figure 10, it can be concluded that the phyllic alteration of the northern part is attributed.

As you can see, the argillic alteration zone in the northern part is marked and is also within the Mesgaran region. In the southern part of the area, the alteration zone is seen as weakly.

### Least Square Fitting (LS-Fit) Method

The method of least squares regression on SWIR bands has been applied to the ASTER satellite data in order to show the spectral properties of hydrothermal alterations. To determine the range of alteration zone of phyllic and argillic indicative minerals such as kaolinite, muscovite, illite, montmorillonite, alunite and pyrophyllite were investigated. According to the indicative clay minerals mentioned above, this band was used



as a model for the study of clay minerals based on the reflection system found in band 4 for minerals such as Kaolinite and muscovite and alunite.

As seen in the image, the range studied does not change to bright pixels. In this method, for detection of alteration, band 9 was also investigated. But the opposite is true of the ratio of SWIR bands to band 9, which is high in chlorite band. The method of least squares regression in relation to band 9, due to the absorption of chlorite in this band, causes the target pixels to darken (Ramezani, 2011). So, after reversing the image in Figure 13, it is achieved.

The accompaniment of these two images can also be indicative of some of the features.

As you know, the main copper mineral chlorite is considered to be the VMS type and the propylitic zone (from the outer porphyry copper zone). This zone is visible in the above image on the southern margin. But it does not have much in its range. To ensure the results of the image are attached

with the image of RGB = 468 and the chlorite in that image are also green, and we can say that in the image, the study area has propylitic alteration including chlorite. And they appear in two almost identical images, and they agree on the subject in the south of region.

**Spectral Angle Mapper (SAM) Method**

In this method, by selecting a mineral zone that assures the presence of the minerals in question, the other regions with an angle of 0.01 in the band of 4, 6 and 8 in the SWIR range were compared with other points. In order to find the areas that are matched with the mineral range of the Mesgaran region to suggest more exploration regions.

With this review, the same points were noted for the angular radius. However, regions with less probability percentages were also found in another image (bright pixels with the highest probability to off pixels with the lowest probability).

In this study, it can be seen that in addition to the Mesgaran region, it is possible to find similar

Figure 14: The Image Obtained from the SAM Method by Selecting the Angle of the Study Area on Other Regions to Display the Anomalous Regions (Red Pixels)

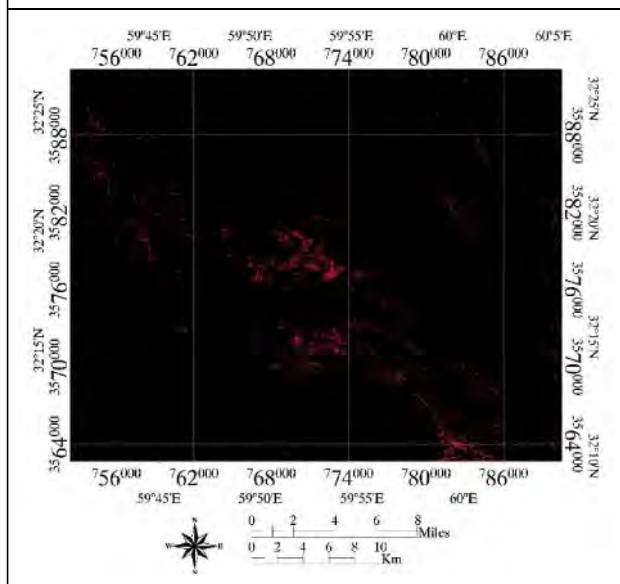
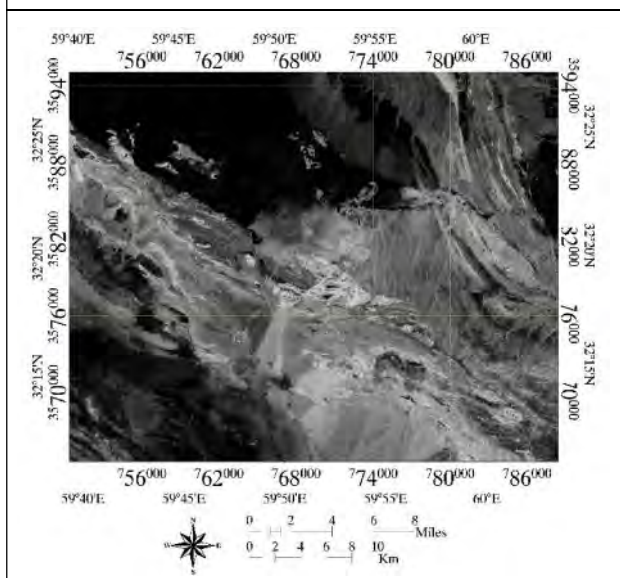


Figure 15: The Image of the Probabilities Derived from the SAM Method for Displaying the Anomalous Areas (Bright Pixels with the Highest Probability to Off Pixels with the Lowest Probability)



cases around this region, which, according to the second phase of exploratory, is partly located in this area, which indicates the desired resolution of this method (Figures 14 and 15).

## CONCLUSION

- Surrounding anomalies can be used to find other surface anomalies in the area, which are similar to the area studied.
- Due to the vast expanse of the exploration area and the availability of accurate information for a small part of the area (Mesgaran mining area), the best approach to potential in the preparatory phase of exploration is remote sensing. Because of the criteria for locating the known region, other regions can be identified as relative. In this research, various methods were used to demonstrate the power of remote sensing in mineral exploration, using ASTER images.
- The methods used include Band Ratios (BR), False Color Combinations (FCC), Least Square Fitting (LS-Fit), Principal Components Analysis (PCA) and finally Spectral Angle Mapper (SAM).
- Each of the mentioned methods has its own results, but the best separation of the region in general was done in the spectral angle mapping method because the level of separation as well as the indexation of the study area was very favorable and high.

## REFERENCES

1. Abbaszadeh M (2010), "Mapping Hydrothermal Alterations Using ASTER Images in Parkam Area, Kerman", *GEOSCIENCES*, Vol. 78.
2. Abbaszadeh M and Hezarkhani A (2010), "Hydrothermal Alteration Mapping Using ASTER Images in Parcam Area, Kerman", *Journal of Earth Sciences*, Vol. 78, pp. 123-128.

3. Abdelaziz R, El-Rahman Y A and Wilhelm S (2018), "Landsat-8 Data for Chromite Prospecting in the Logar Massif, Afghanistan", *Heliyon*, Vol. 4, No. 2, p. e00542.
4. Agharezaei M and Hezarkhani A (2016), "Delineation of Geochemical Anomalies Based on Cu by the Boxplot as an Exploratory Data Analysis (EDA) Method and Concentration-Volume (CV) Fractal Modeling in Mesgaran Mining Area, Eastern Iran", *Open Journal of Geology*, Vol. 6, No. 10, p. 1269.
5. Amer R, Kusky T and Ghulam A (2010), "Lithological Mapping in the Central Eastern Desert of Egypt Using ASTER Data", *Journal of African Earth Sciences*, Vol. 56, Nos. 2-3, pp. 75-82.
6. Aqanabati A (2009), *Geology of Iran*, IRAN: Ministry of Industries and Mines: Geological Survey of Iran.
7. Arivazhagan S and Anbazhagan S (2017), "ASTER Data Analyses for Lithological Discrimination of Sittampundi Anorthositic Complex, Southern India".
8. Asadzadeh S and de Souza Filho C R (2016), "A Review on Spectral Processing Methods for Geological Remote Sensing", *International Journal of Applied Earth Observation and Geoinformation*, Vol. 47, pp. 69-90.
9. Bransden B H and Joachain C J (2003), *Physics of Atoms and Molecules*, Pearson Education India.
10. Crosta A, De Souza Filho C, Azevedo F and Brodie C (2003), "Targeting Key Alteration Minerals in Epithermal Deposits in Patagonia, Argentina, Using ASTER Imagery and Principal Component Analysis", *International Journal of Remote Sensing*, Vol. 24, No. 21, pp. 4233-4240.
11. Dhara M, Sengar V K, Chatteraj S L and Bhattacharjee S (2017), "Mapping of Alteration Zones in Mineral Rich Belt of South-East Rajasthan Using Remote Sensing Techniques", *World Academy of Science, Engineering and Technology, International Journal of Environmental, Chemical, Ecological, Geological and Geophysical Engineering*, Vol. 11, No. 2, pp. 154-158.
12. Esmaeeli M, Tabaei M and Asadiharooni H (2012), *Remote Sensing Study (ASTER & TM) and Geology of Southwest Meyme Iron Ore Deposit, IRAN*, Paper Presented at the 31<sup>st</sup> Symposium of Geosciences, Tehran, IRAN.
13. Ezzati A, Mehrnia R and Ajayebi K (2014), "Detection of Hydrothermal Potential Zones Using Remote Sensing Satellite Data in Ramand Region, Qazvin Province, Iran", *Journal of Tethys*, Vol. 2, No. 2, pp. 93-100.
14. Ferrier G, White K, Griffiths G, Bryant R and Stefouli M (2002), "The Mapping of Hydrothermal Alteration Zones on the Island of Lesbos, Greece Using an Integrated Remote Sensing Dataset", *International Journal of Remote Sensing*, Vol. 23, No. 2, pp. 341-356.
15. Gahlan H and Ghrefat H (2018), "Detection of Gossan Zones in Arid Regions Using Landsat 8 OLI Data: Implication for Mineral Exploration in the Eastern Arabian Shield, Saudi Arabia", *Natural Resources Research*, Vol. 27, No. 1, pp. 109-124.

- 
16. Garg V, Kumar A S, Aggarwal S, Kumar V, Dhote P R, Thakur P K and Muduli P R (2017), "Spectral Similarity Approach for Mapping Turbidity of an Inland Waterbody", *Journal of Hydrology*, Vol. 550, pp. 527-537.
  17. Ghannadpoor S S, Hezarkhani A and Farahshan E (2012), "Identification and Separation of Hydrothermal Alteration Zones in the Kerman Province of Parcam Using Satellite Data of Aster", Paper Presented at the First Iranian Geological Survey, Kerman.
  18. Gómez-Palacios D, Torres MA and Reinoso E (2017), "Flood Mapping Through Principal Component Analysis of Multitemporal Satellite Imagery Considering the Alteration of Water Spectral Properties Due to Turbidity Conditions", *Geomatics, Natural Hazards and Risk*, Vol. 8, No. 2, pp. 607-623.
  19. Guo H, Huang Q, Li X, Sun Z and Zhang Y (2013), "Spatiotemporal Analysis of Urban Environment Based on the Vegetation-Impervious Surface-Soil Model", *Journal of Applied Remote Sensing*, Vol. 8, No. 1, pp. 084-597.
  20. Gupta R P (2017), *Remote Sensing Geology*, Springer.
  21. Hasan E, Fagin T, El Alfy Z and Hong Y (2016), "Spectral Angle Mapper and Aeromagnetic Data Integration for Gold-Associated Alteration Zone Mapping: A Case Study for the Central Eastern Desert Egypt", *International Journal of Remote Sensing*, Vol. 37, No. 8, pp. 1762-1776.
  22. Hassanipak A A and Sharafeddin M (2005), *Exploration Data Analysis*, Vol. 1, Tehran University Press, Tehran.
  23. Hereher M E and Abdullah S E (2017), "Lithologic Mapping of Aja Granitic Batholiths, Ha'il, Saudi Arabia, Using Remote Sensing", *Arabian Journal of Geosciences*, Vol. 10, No. 14, p. 313.
  24. Hooshyari N (2005), *Separation of Alteration Zones in Relation to Possible Mineralization of Gold and Copper Zofre Area Using Satellite Data ASTER*, (BSc), Isfahan University of Technology.
  25. Kalinowski A and Oliver S (2004), "ASTER Mineral Index Processing Manual", *Remote Sensing Applications, Geoscience Australia*, Vol. 37, p. 36.
  26. Liu J G and Mason P J (2013), *Essential Image Processing and GIS for Remote Sensing*, John Wiley & Sons.
  27. Manuel R, Brito M D G, Chichorro M and Rosa C (2017), "Remote Sensing for Mineral Exploration in Central Portugal", *Minerals*, Vol. 7, No. 10, p. 184.
  28. Markovskiy N (2014), "Drop-in Acceleration of GNU Octave".
  29. Masoumi F, Eslamkish T, Honarmand M and Abkar A A (2017), "A Comparative Study of Landsat 7 and Landsat 8 Data Using Image Processing Methods for Hydrothermal Alteration Mapping", *Resource Geology*, Vol. 67, No. 1, pp. 72-88.
  30. Mohammadi S, Vosoughi A M, Pourmoafi S, Emami M and Khatib M (2007), "Petrography, Geochemistry, Genesis and Tectonic Setting of Mesgaran Area Granitoids (South-East of Birjand)".
  31. Obata K, Tsuchida S, Yamamoto H and Thome K (2017), "Cross-Calibration Between ASTER and MODIS Visible to Near-Infrared Bands for Improvement of ASTER Radiometric Calibration", *Sensors*, Vol. 17, No. 8, p. 1793.
-

- 
32. Padró J-C, Pons X, Aragonés D, Díaz-Delgado R, García D, Bustamante J and Cristóbal J (2017), "Radiometric Correction of Simultaneously Acquired Landsat-7/ Landsat-8 and Sentinel-2A Imagery Using Pseudoinvariant Areas (PIA): Contributing to the Landsat Time Series Legacy", *Remote Sensing*, Vol. 9, No. 12, p. 1319.
33. Ramezanali A, Mansouri E and Feizi F (2017), "Integration of Aeromagnetic Geophysical Data with Other Exploration Data Layers Based on Fuzzy AHP and CA Fractal Model for Cu-Porphyry Potential Mapping: A Case Study in the Fordo Area, Central Iran", *Bollettino di Geofisica Teorica ed Applicata*, Vol. 58, No. 1.
34. Ramezani M (2011), *Remote Sensing Studies Using ENVI Software about Midok Range in Kerman Province*, (BS).
35. Ran L, Zhang Y, Wei W and Zhang Q (2017), "A Hyperspectral Image Classification Framework with Spatial Pixel Pair Features", *Sensors*, Vol. 17, No. 10, p. 2421.
36. Ranjbar H, Shahriari H and Honarmand M (2004), "Integration of ASTER and Airborne Geophysical Data for Exploration of Copper Mineralization: A Case Study of Sar Cheshmeh Area", Paper Presented at the Proceedings of 20th Congress, International Society for Photogrammetry and Remote Sensing, Istanbul.
37. Razmi M, Asgari H M, Sohrab A D, Nazemosadat S M J and Khazaei S H (2017), "Monitoring Oscillations Coastline of Dayyer City During the El Niño and La Niño Using OIF Utility Index".
38. Robert A S (2007), "Remote Sensing: Models and Methods for Image Processing", by Elsevier Inc. All Rights Reserved, pp. 300-304.
39. Safari M, Maghsoudi A and Pour A B (2017), "Application of Landsat-8 and ASTER Satellite Remote Sensing Data for Porphyry Copper Exploration: A Case Study from Shahr-e-Babak, Kerman, South of Iran", *Geocarto International*, pp. 1-16.
40. Schott J R (2007), *Remote Sensing: The Image Chain Approach*, Oxford University Press on Demand.
41. Shirazi A (2016), *Lithology and Economic Geology Surveys of Copper in Mesgaran (South Khorasan)*, (BS), Amirkabir University of Technology.
42. Shirazi A, Hezarkhani A, Shirazy A and Shahrood I (2018), "Remote Sensing Studies for Mapping of Iron Oxide Regions, South of Kerman, IRAN", *International Journal of Science and Engineering Applications*, Vol. 7, No. 4, pp. 45-51.
43. Shirazi A, Hezarkhani A, Shirazy A and Shahrood I (2018), "Exploration Geochemistry Data-Application for Cu Anomaly Separation Based on Classical and Modern Statistical Methods in South Khorasan, Iran".
44. Soe M, Kyaw T A and Takashima I (2005), "Application of Remote Sensing Techniques on Iron Oxide Detection from ASTER and Landsat Images of Tanintharyi Coastal Area, Myanmar".
45. Vincent R K (1997), *Fundamentals of Geological and Environmental Remote Sensing*, Vol. 366, Prentice Hall Upper Saddle River, NJ.
46. Wang G, Du W and Carranza E J M (2017), "Remote Sensing and GIS Prospectivity
-



- Mapping for Magmatic-Hydrothermal Base- and Precious-Metal Deposits in the Honghai District, China”, *Journal of African Earth Sciences*, Vol. 128, pp. 97-115.
47. Yao K, Pradhan B and Idrees M O (2017), “Identification of Rocks and their Quartz Content in Gua Musang Goldfield Using Advanced Spaceborne Thermal Emission and Reflection Radiometer Imagery”, *Journal of Sensors*.
48. Zarjabad H H, Zareie A, Harchegani T B and Farjami M (2015), “Archaeological Investigation of Metal Smelting in Eastern Iran Case Study: Mesgaran Area”, One of the Most Ancient Metal Smelting Plants in South Khorasan.
49. Zhao B, Shao G, Fan B, Zhao W, Xie Y and Zhang R (2015), “Synthesis of Flower-Like CuS Hollow Microspheres Based on Nanoflakes Self-Assembly and their Microwave Absorption Properties”, *Journal of Materials Chemistry A*, Vol. 3, No. 19, pp. 10345-10352.